

Figure 3. DSC thermogram of polymer liquid crystal II, scanned at +40 °C/min after quenching from 250 °C.

and 35 000 g/mol. The GPC trace was obtained for II in ethyl acetate (99.9+%, HPLC grade, Aldrich) at a column temperature of 40 °C and a flow rate of 0.84 mL/min. The linearity between the logarithm of molecular weight and retention volume for the polystyrene standards listed above justifies the reliability of the molecular weight distribution obtained for II from the GPC measurement; there should be no concern with the total exclusion of polymer solutes up to a molecular weight of 35 000 g/mol.

Acknowledgment. The authors thank K. L. Marshall of the Laboratory for Laser Energetics, University of Rochester, for his technical assistance and Dr. Abraham Warshawsky of the Weizmann Institute of Science, Rehovot, Israel, for helpful discussions. The work reported here was supported by the New York State Center for Advanced Optical Technology at the University of Roch-

ester. The other sources of support came from the National Science Foundation under Grant CBT-8714924 and from the Army Research Office. Such support does not imply endorsement of the content by any of the above parties.

References and Notes

- (1) Ciferri, A.; Krigbaum, W. R.; Meyer, R. B. *Polymer Liquid Crystals*; Academic: New York, 1982.
- (2) Blumstein, A. *Liquid Crystalline Order in Polymers*; Academic: New York, 1978.
- (3) Platé, N. A. *Liquid Crystal Polymers I and II/III*; Springer-Verlag: Berlin, 1984; Vols. 59-61.
- (4) Chapoy, L. L. *Recent Advances in Liquid Crystalline Polymers*; Elsevier: London, 1985.
- (5) Lipatov, Yu. S.; Tsukruk, V. V.; Shilov, V. V. *J. Macromol. Sci., Rev. Macromol. Chem. Phys.* **1984**, *C24*, 173.
- (6) Varshney, S. K. *J. Macromol. Sci., Rev. Macromol. Chem. Phys.* **1986**, *C26*, 551.
- (7) Regen, S. L. *Angew. Chem., Int. Ed. Engl.* **1979**, *18*, 421.
- (8) Ford, W. T.; Tomoi, M. *Adv. Polym. Sci.* **1984**, *55*, 49.
- (9) Chen, S. H.; Maa, Y. F. *Macromolecules* **1988**, *21*, 904.
- (10) Keller, P. *Macromolecules* **1984**, *17*, 2937.
- (11) Pfeffer, P. E.; Foglia, T. A.; Barr, P. A.; Schmeltz, I.; Silbert, L. S. *Tetrahedron Lett.* **1972**, 4063.
- (12) Shaw, J. E.; Kuerth, D. C.; Sherry, J. J. *Tetrahedron Lett.* **1973**, 689.
- (13) Pfeffer, P. E.; Silbert, L. S. *J. Org. Chem.* **1976**, *41*, 1373.
- (14) Tiecco, M.; Testaferri, L.; Tingoli, M.; Chianelli, D.; Montanucci, M. *J. Org. Chem.* **1983**, *48*, 4795.
- (15) Idoux, J. P.; Madenwald, M. L.; Garcia, B. S.; Chu, D. L. *J. Org. Chem.* **1985**, *50*, 1876.
- (16) Shaw, J. E.; Kuerth, D. C.; Swanson, S. B. *J. Org. Chem.* **1976**, *41*, 732.
- (17) Pham, Q. T.; Petiaud, R.; Llauro, M. F.; Waton, H. *Proton and Carbon NMR Spectra of Polymers*; Wiley: New York, 1984; Vol. III, p 455.
- (18) van Meter, J. P.; Klanderman, B. H. *Mol. Cryst. Liq. Cryst.* **1973**, *22*, 285.
- (19) Hassner, J.; Alexanian, V. *Tetrahedron Lett.* **1978**, 4475.

Molecular Orientation Profiles in an Injection-Molded Liquid Crystalline Copolyester Characterized by Fourier Transform Infrared Attenuated Total Reflection Dichroism

Abolhassan Pirnia and Chong Sook Paik Sung*

Institute of Materials Science, Department of Chemistry, The University of Connecticut, 97 North Eagleville Road, Storrs, Connecticut 06268. Received October 13, 1987

ABSTRACT: FT-IR ATR dichroism, averaging about 5 μm in depth, has been used to obtain the orientation profiles in injection-molded plaques of a thermotropic main-chain liquid crystalline polymer. The polymer is a copolyester containing 58 mol % of hydroxybenzoic acid (HBA) and 42 mol % 2,6-hydroxynaphthoic acid (HNA). Orientation functions were measured at eight positions as a function of distance from the end gate and at four positions in the thickness direction, providing a complex, three-dimensional orientation profile. Orientation profiles are similar for both HBA and HNA bands, a trend which attests to a random structure for this copolyester. Orientation functions along the surface plane show transverse orientation at a position closest to the gate due to the radial character of the flow in this region. Orientation functions in the thickness direction indicate that the chains are mostly planar with respect to the mold wall, especially on the skin. Based on the orientation data on the subskin, "the orientability parameter" was estimated to be close to unity, a value suggesting the enhanced orientational capabilities of these materials. The strong orientation of molecules in the skin layer generally decreases as one probes along the thickness direction. In the core layer, little orientation is observed in either the flow direction or the thickness direction for the first half of the mold, indicating random orientation probably due to the persistence of the polydomain structure in the molding operation. These experimental results are in agreement at least qualitatively with the predictions based on mold filling of short fiber-filled thermoplastics and structural rearrangements in liquid crystalline polymers.

Introduction

Recently, thermotropic main-chain liquid crystalline polymers (LCPs) have received a great deal of attention due to the possibility of melt processing these materials

into products with exceptional physical properties. Researchers at Eastman Kodak were first to report on an aromatic-aliphatic copolyester made of *p*-hydroxybenzoic acid (HBA) and poly(ethylene terephthalate) (PET).^{1,2}

Calundann and Jaffe prepared all aromatic copolyesters based on *p*-hydroxybenzoic acid (HBA) and 2,6-hydroxynaphthoic acid (HNA).^{3,4} The presence of the aliphatic sequence in the HBA/PET chain imparts some flexibility while the HBA/HNA chains are essentially rigid, as probed by NMR.⁵

Comprehensive characterization of the solid-state molecular structure, morphology, and orientation in these LCPs is necessary for better understanding their physical and mechanical properties. Blackwell et al. have shown that the X-ray diffraction data for the fibers drawn from the HBA/HNA copolymer are consistent with a structure made up of oriented, extended chains of completely random monomer sequence.^{6,7} Furthermore, they showed that the 1,4- and 2,6-linkages of the planar aromatic and ester groups lead to an extended conformation with bonds that are approximately parallel to the chain axis.⁸ X-ray diffraction and thermal analysis by Blundell indicated the presence of microcrystals that were too small to give clear X-ray lines in the quenched solidified HBA/HNA polymer. It was proposed that this phenomenon was due to the very low surface energy characteristic of the nematic chain morphology.⁹ Using TEM, Donald and Windle made similar observations and referred to such microcrystals as "ordered entities" due to the lack of full three-dimensional crystalline order.^{10,11}

Injection molding of short fiber-filled thermoplastic polymers is generally known to introduce anisotropic structures which vary from location to location as well as along the thickness direction and which are often layered.¹² Injection-molded plaques of thermotropic main-chain LCPs have also exhibited a highly anisotropic behavior. For example, Jackson and Kuhfuss measured a flexural modulus that was ten times greater in the flow direction than transverse to the flow direction.¹³ Ophir and Ide measured a flexural modulus as a function of test angle that exhibited a much higher anisotropy than glass-filled polybutylene terephthalate.¹⁴ A skin/core morphology, with distinct molecular orientation, has been proposed as the source of the anisotropy in physical properties. Using wide-angle X-ray scattering and electron microscopy, Baird and co-workers have studied the morphological textures in end-gated injection-molded plaques of HBA/PET and have found a highly oriented skin layer and a less oriented core layer.¹⁵ Sawyer and Jaffe have also studied these morphological textures for a host of HBA/HNA type thermotropic copolyesters using microscopic techniques¹⁶ and observed complex, yet regular, variations of molecular orientation in thick extrudates and molded parts. The skin layer was found to have a molecular orientation parallel to the flow direction whereas the core layer showed little or no orientation and was relatively featureless. Baer and co-workers proposed a hierarchical structure for injection-molded plaques of HBA/HNA copolymer.¹⁷ Wide-angle X-ray scattering and scanning electron microscopy showed a skin layer that was oriented parallel to the flow direction while the core layer was oriented transverse to the flow.

It is clear then that the anisotropy in physical properties in molded thermotropic main-chain LCPs is related to the existence of a complex morphological texture. The unique morphological texture of these materials is a function of their many small domains with a high degree of local ordering, which make them highly susceptible to influence by the nonisothermal flow fields involved in injection molding. Elucidation of these morphological textures in terms of a composite orientation distribution should be helpful in understanding the rheological behavior of these

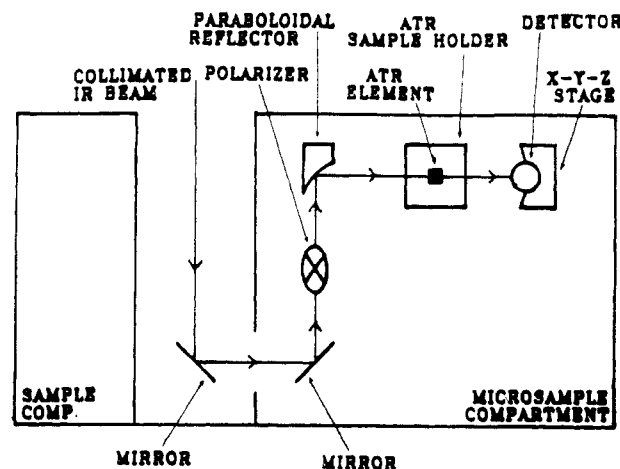


Figure 1. Schematic of the new FT-IR ATR dichroism setup in the microsample compartment of a Nicolet 60 SX instrument.

materials as well as predicting the mechanical properties of the final product. Therefore, we measured molecular orientation on an injection-molded thermotropic copolyester of HBA/HNA type as a function of the distance from the end gate and of the thickness. The polymer and the plaque geometry in our study were the same as those studied by Weng et al.,¹⁷ except that in their studies the thickness of the plaque was only half that of our specimen. Their study focused only on the morphological features observed as a function of the thickness, while we characterized their structures also as a function of the distance from the end gate in order to interpret the experimental results in view of the predictions based on short-fiber orientation in injection molding.

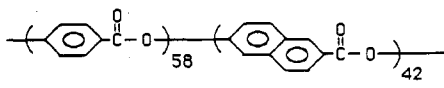
The experimental technique used is FT-IR attenuated total reflection (ATR) dichroism which has been developed in our laboratory, using a special ATR crystal and ATR attachment,^{18,19} which resulted in an improved quality of the spectra. The important features of this ATR setup are a double-beveled symmetrical crystal and a C-clamp sample holder to allow the sample to be rotated without disassembling and reassembling operations, which would change the contact area between the polymer and the ATR crystal. Under our experimental conditions, ATR dichroism can probe about 5 μm in depth.

Experimental Section

ATR Dichroism. A new ATR attachment was built and installed as a semipermanent ATR dichroism setup in the microsample compartment of the FT-IR spectrometer (Nicolet 60SX). As illustrated in Figure 1, the main IR beam is directed by two flat mirrors to travel parallel to the compartment wall, before passing through a Ge double-diamond polarizer (Harrick Scientific). The collimated beam is then focused on the entrance face of the ATR element by using a 90° off-axis parabolic reflector (Melles Griot). By carrying out a simple experiment in which the plane of polarization of a second polarizer was varied with respect to the first, it was found that the rotation of the plane of polarization due to reflection from the parabolic reflector does not occur within experimental error and that the polarization efficiency is 98%.²⁰ The specially designed ATR element was made of KRS-5 (Harrick Scientific) with the dimensions of 20 mm \times 20 mm \times 2 mm.

The liquid nitrogen cooled MCT-A detector was placed close to the exit face of the ATR element. Maximum signal intensity, as observed on an oscilloscope, was obtained by carefully positioning the detector with an x-y-z stage (Daedal, Inc.). This arrangement led to a signal amplification of at least five times that of the usual ATR setup in the main sample compartment and improved the signal-to-noise ratio appreciably with a maximum noise of 2% in the ATR spectra. ATR spectra, at an

Chart I
Chemical Structure and Some Characteristics of Injection
Molded HBA/HNA 58/42 Copolyester

			
m.p. (°C)	η^* inh (dl/g)	melt temperature (°C)	mold temperature (°C)
247	5.1	252	100

* at 60 °C in 0.1 % solution of pentafluorophenol

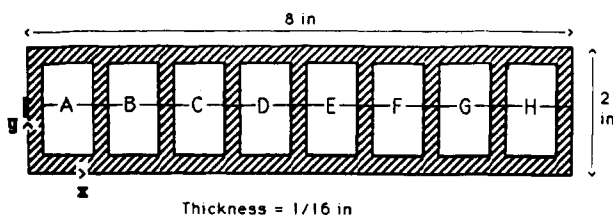


Figure 2. Schematic of injection-molded plaque of the HBA/HNA 58/42 copolyester showing the end gate and the sample positions A-H.

incidence angle of 45°, were collected in groups of 50 scans and were coadded with high correlation for a total of 400 scans. Spectral resolution was 2 cm⁻¹. Sample spectra were ratioed against background spectra corresponding to each polarization and sample rotation.

Materials. A wholly aromatic copolyester consisting of 58 mol % *p*-hydroxybenzoic acid (HBA) and 42 mol % 2,6-dihydroxynaphthoic acid (HNA) was used in this study, herein designated as HBA/HNA 58/42. This polymer softens at 222 °C and becomes fluid at 247 °C.²¹ It has an inherent viscosity of 5.1 dL/g at 60 °C in 0.1% solution of pentafluorophenol, as summarized in Chart I. End-gated, rectangular, injection-molded plaques were generously supplied by Dr. S. Garg of Celanese. The plaques had the dimensions 8 in. × 2 in. × 1/16 in. (203.2 mm × 50.8 mm × 1.6 mm). The processing conditions were 252 °C for the melt temperature and 100 °C for the mold temperature.

Sample Preparation for Analyses. The plaques were sectioned into eight pairs of squares (18 mm × 18 mm) by using a band saw. They were labeled from "A" to "H" as a function of distance from gate, "A" being the closest to the gate. Consecutive pairs were separated from one another by 7 mm. Figure 2 shows a schematic of the sectioned plaques. Four thickness positions were studied. The skin layer was that in contact with the mold wall. The subskin, intermediary, and core layers were located at 98%, 75%, and 50% of the total thickness, respectively. Thickness reduction was done with an end-cutter on a milling machine with an accuracy of ±1 mil and was checked with a micrometer for each position. The possibility of milling-induced orientational effects was tested by FT-IR ATR dichroism. Identical pairs were unidirectionally milled in different directions. It was found that the measured orientation functions fell within the experimental error range of multiple sampling runs.

All surfaces were cleaned with acetone before FT-IR ATR dichroism measurements.

IR Band Assignment. FT-IR spectra of the homopolymers of HBA and HNA were obtained in transmission mode by the KBr pellet method and are represented in Figure 3. For our analyses, we chose four well-separated IR bands at 1628, 1502, 1468, and 1412 cm⁻¹. These bands are known to be parallel bands associated with the skeletal vibrations of the benzene and naphthalene rings in the polymer.²² Two of these bands (1628 and 1468 cm⁻¹) are only due to the HNA component while the other two (1502 and 1412 cm⁻¹) are mostly due to HBA with some contribution from HNA.

Molecular Orientation Measurements. A polymer film surface exhibits three spatial absorbances, A_x , A_y , and A_z , which are related to the ATR dichroic spectra band intensities for the

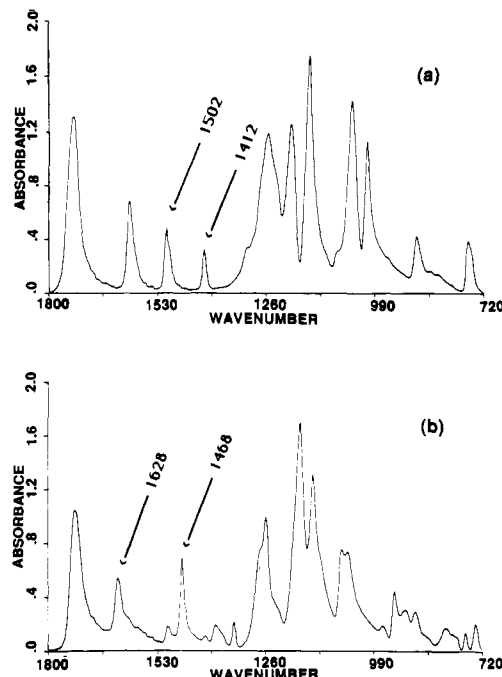


Figure 3. Transmission IR spectra of the HBA polyester (a) and of the HNA polyester (b).

transverse electric (TE) and transverse magnetic (TM) waves; A_{TE_x} , A_{TM_x} , A_{TE_y} , and A_{TM_y} according to the following equations:²³

$$A_{TE_x} = \alpha A_x$$

$$A_{TM_x} = \beta A_y + \gamma A_z$$

$$A_{TE_y} = \alpha A_y$$

$$A_{TM_y} = \beta A_x + \gamma A_z$$

where α , β , and γ are constants determined by the refractive indices of the sample (n_{polymer}) and the crystal (n_{crystal}) and the angle of incidence (θ). For 45° incidence, the constants are given by

$$\alpha = \frac{4n^2}{(1-n^2)(1-2n^2)^{1/2}}$$

$$\beta = \frac{4n^2(1-2n^2)^{1/2}}{(1-n^2)^2}$$

$$\gamma = \frac{4n^2}{(1-n^2)^2(1-2n^2)^{1/2}}$$

where $n = n_{\text{polymer}}/n_{\text{crystal}}$.

The refractive index of this copolymer was estimated by simple addition of the functional group contributions to be 1.65.²⁴ Based on this rough estimate, α , β , and γ were calculated to be 27.2, 1.1, and 53.3, respectively.

For uniaxial liquid crystalline phases, assuming that the transition dipole moment is parallel to the long axis of the molecule, an orientation function can be defined as

$$f = (D - 1)/(D + 2)$$

where D is the dichroic ratio.²⁵ For a perfectly aligned (monodomain) uniaxial liquid crystalline phase, if the orientation function is measured parallel to the nematic director, it is equivalent to the order parameter (S) of the liquid crystal

$$S = \frac{1}{2} \langle 3 \cos^2 \theta - 1 \rangle$$

where θ is the angle between the long axis of the molecule and the optic axis and the angled brackets symbolize an average of all molecules.²⁶

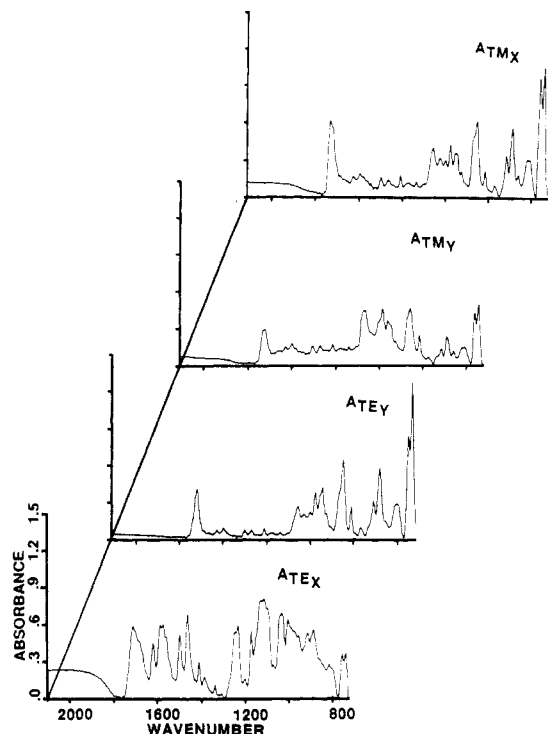


Figure 4. Four FT-IR ATR dichroic spectra obtained from the skin surface of the HBA/HNA 58/42 copolyester at position D.

We define x , y , and z as the flow direction, the transverse to flow direction, and the thickness direction, respectively. Dichroic ratios, $D_{xy} = A_x/A_y$ and $D_{zz} = A_x/A_z$, are used to calculate the orientation functions, as defined by

$$f_{xy} = (D_{xy} - 1)/(D_{xy} + 2)$$

$$f_{zz} = (D_{zz} - 1)/(D_{zz} + 2)$$

For perfect flow direction orientation, f_{xy} is equal to 1.0, whereas for perfect transverse orientation it is equal to -0.5. If the molecules are perfectly planar, f_{zz} is equal to 1.0, and if they lie

with their long axis in the thickness direction, it takes on a value of -0.5.

Results and Discussion

Figure 4 illustrates representative FT-IR ATR spectra obtained from the skin layer at position "D" by rotating the sample with respect to TE and TM polarizations. Strong dichroism is observed for the parallel bands at 1628, 1502, 1468, and 1412 cm^{-1} . The good signal-to-noise ratio allowed us to measure dichroic ratios from which the orientation functions f_{xy} and f_{zz} were calculated.

The orientation functions for the combination bands at 1502 and 1412 cm^{-1} and the pure HNA bands at 1628 and 1468 cm^{-1} are presented in Figure 5. These show the orientation development as a function of distance from the gate in the skin layer. In order to assess the experimental error in these types of measurements, the ATR spectra was taken three times for each location by reassembling the sample in the ATR attachment. The error bars represent standard deviations from three separate spectral analyses, which are small compared to the observed orientation at different positions. Therefore, we can conclude that changes in orientation as a function of position are real.

The orientation profile is generally of the same shape but differs in magnitude for different bands. This suggests that the assumption of a zero angle between the transition moment vector for the vibrations and the chain axis is not strictly correct. However, since we were interested in relative orientations in three dimensions for a given band, we saw no need to make any corrections in this regard. Orientation profiles are similar for mostly HBA bands (1502, 1412 cm^{-1}) and HNA bands (1628, 1468 cm^{-1}), which seems to attest to the random structure of this copolyester. A similar conclusion was reached by X-ray studies.^{6,7} The magnitudes of the orientation functions are highest for the band at 1468 cm^{-1} with an average value for the pseudo-plateau ("B" to "H") of 0.77 and 0.88 for f_{xy} and f_{zz} , respectively. The band at 1412 cm^{-1} exhibits the lowest orientation functions and the other two bands are comparable in magnitude.

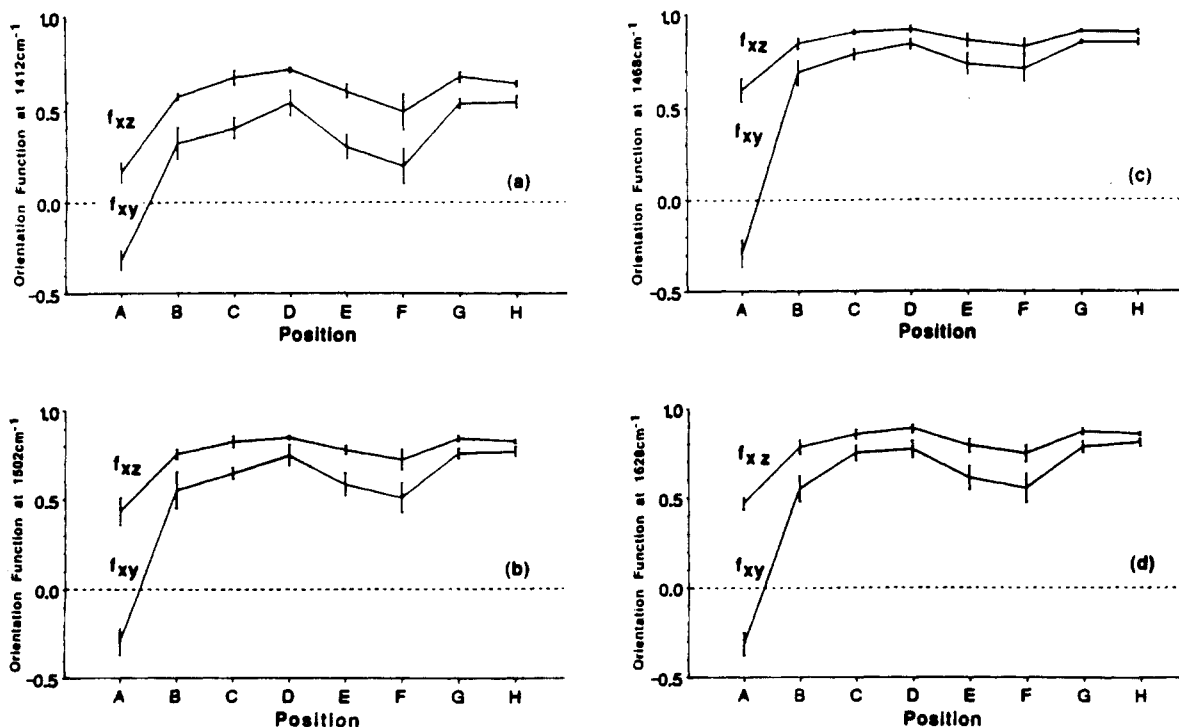


Figure 5. Orientation functions (f_{xy} and f_{zz}) of the skin layer at different positions from the end-gate, monitored at 1412 (a), 1502 (b), 1468 (c), and 1628 cm^{-1} (d).

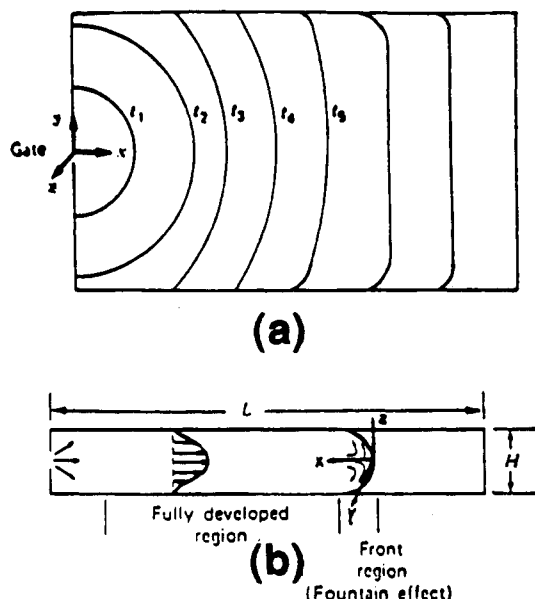


Figure 6. Mold-filling process for an end-gated rectangular cavity: (a) x - y plane view of the flow front advance; (b) x - z plane cross-sectional view of the velocity profiles (from ref 27).

It is useful here to present a schematic of the mold-filling process for an end-fed rectangular cavity. Figure 6 is taken from a recent paper by Gogos et al. which shows the position and the shape of the melt front at different times during the filling stage.²⁷ It can be seen that the melt front is initially circular and starts to flatten out when the melt radius becomes equal to the half-width of the mold. Injection molding involves transient, nonisothermal flow over a wide range of shear rates. Up to moderate flow rates, however, mold filling is orderly. As depicted in the picture, the flow is radial near the gate, but further away it is characterized by a dominant x -component flow and at the advancing front a strong z -component flow prevails. In discussing the orientation results with respect to the flow fields that might be responsible for them, we assume that molecular relaxation is negligible within the time required for the plaque to solidify. This is a good assumption given the long relaxation times for liquid crystalline polymers, as compared to isotropic materials.²⁸ At position "A" which is the closest to the gate, the average orientation of the chains in the xy plane is transverse to the flow direction. In this region, the melt front is circular. The melt radius becomes equal to the half-width of the mold just before position B. At position B, the melt front starts to flatten out and thus flow direction orientation is observed. As the melt front becomes more flat (C and D) higher molecular orientation is observed. Positions E and F exhibit lower orientation functions. This might be due to flow instabilities in the front region in these positions. A recovery of molecular orientation is observed toward the end of the mold, G and H. High orientation functions in the xz plane show that the chains lie preferentially in the xy plane; i.e., they are planar with respect to the mold wall. This planar orientation has been observed by others on thin oriented films of a different thermotropic polyester using transmission polarized IR spectroscopy.²⁹

Orientation functions for the subskin, intermediary, and core layers are presented in Figure 7 for the band at 1468 cm^{-1} . While the general shapes of the orientation profiles for other bands are similar to the 1468-cm^{-1} band, we chose to show the profiles for this band because it exhibited the highest values in the skin layer.

In the subskin layer, position A exhibits slight transverse orientation in the xy plane with a value much lower than

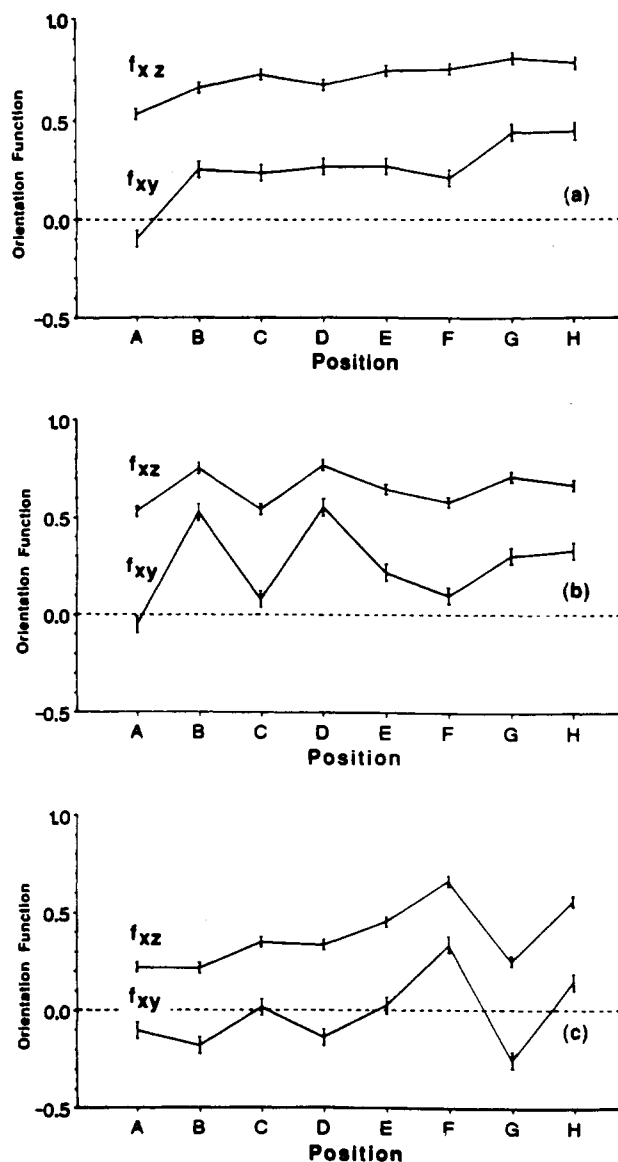


Figure 7. Orientation functions (f_{xy} and f_{xz}) of the subskin layer (a), the intermediary layer (b), and the core layer (c) at different locations from the end gate monitored at 1468 cm^{-1} .

that for the skin layer. Moderate values of flow direction orientation are observed with an average value for the pseudoplateau (B-F) of 0.25. This flow direction orientation increases to a value of 0.44 toward the end of the mold, G and H. Low absorbances in the thickness direction also point out that the chains are mostly planar in this layer. This leads to relatively high f_{xz} values with a profile that is greater than the xy orientation function. By comparison of these values of orientation to those obtained in the skin layer, it can be concluded that the flow field responsible for this thickness layer is less orienting in the xy plane than the flow in the skin layer.

The orientation functions in the intermediary layer exhibit erratic behavior in the first half of the mold. At position A, chains are very slightly transverse to the flow direction in the xy plane but less so than in the previous layers. Positions B and D show values of 0.53 and 0.55 for the xy orientation functions, respectively, which are larger than the corresponding values for the subskin layer. The rest of the positions exhibit flow direction orientation (f_{xz} values) lower than those of the subskin layer. The same type of recovery of molecular orientation is observed toward the end of the mold (G and H) for this layer as observed in the previous layers. The orientation profile

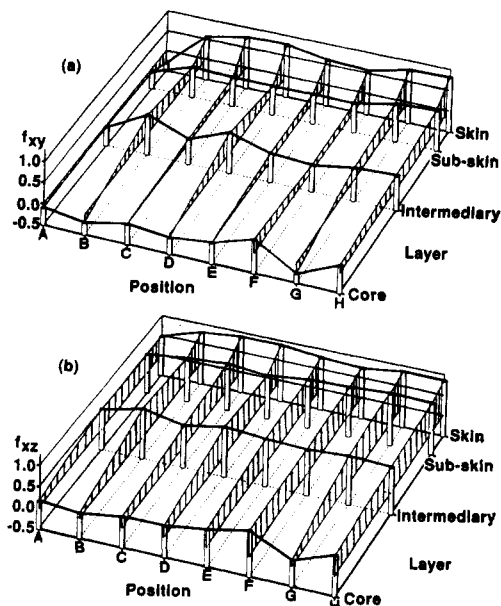


Figure 8. Three-dimensional orientation profiles of f_{xy} (a) and f_{zz} (b) plotted as a function of the thickness layer and of the location from the end gate monitored at 1628 cm^{-1} .

in the xz plane follows that for the xy plane but with greater magnitudes as in the subskin layer. Given these orientation profiles, it may be deduced that a flow field may not be decisive on the average in producing a homogeneous orientation in the first half of the mold. The transient structure and heat transfer as a function of distance from the gate could produce such orientation profiles. This behavior will be discussed in the next section from the point of view of flow analyses.

The smallest extent of orientation has been observed in the core layer, even though some erratic behavior is observed toward the end of the mold. The orientation function in the xy plane changes from 0.33 to -0.25 to 0.14 for positions F, G, and H, respectively. Position A exhibits a higher transverse orientation f_{xy} than the intermediary layer with a value comparable to the subskin layer. Intermediate positions show either slightly transverse or close to isotropic orientations. The absorbances in the thickness direction are low and the f_{zz} profile follows that of f_{xy} closely. The flow field in the core layer seems to influence the chains weakly into a transverse orientation in the first half of the mold. These small f_{xy} and f_{zz} values in the first half of the mold suggest an almost random configuration of the molecules, probably due to the presence of polydomains.

The composite picture of molecular orientation development in three dimensions, as a function of distance from the gate and the thickness direction, is illustrated for the 1628-cm^{-1} band in Figure 8. The experimental points are connected by straight lines and the differences from the isotropic plane at an orientation function of zero are highlighted for visual comparison. In using straight lines, we do not mean to imply continuity of molecular orientation, especially in the thickness direction, as there must be boundaries between different flow fields responsible for these layers, and in fact, several boundaries are quite visible. On the contrary, this figure is meant to illustrate the complexity and heterogeneity of molecular orientation in these molded plaques, which might be elucidated by modeling based on fluid mechanics.

Interpretation of Results in View of Flow Analyses.

In order to understand the flow mechanisms responsible for such layers and orientation profiles, it is necessary to

know the structural development of liquid crystalline polymers in different flow fields.

According to Onogi and Asada,³⁰ the internal structure of liquid crystalline materials is based on the existence of a polydomain structure. A director is associated with each domain and an order parameter S (defined in the Experimental Section) can be calculated which is characteristic of the material under investigation. This director varies from domain to domain and in an unaligned sample, the overall director orientation is isotropic. This polydomain structure can be disrupted depending upon the characteristics of the flow. For a lyotropic LCP, undergoing shear flow, Horio observed the breaking up of the polydomain structure into smaller ($1\text{--}10\text{ }\mu\text{m}$) spherical domains which rotated as they flowed.³¹ He did not observe any birefringence, indicating the absence of macroscopic orientation. Onogi, White, and Fellers found that intense shearing could break up the polydomain structure into a monodomain phase.³² For elongational flow, they reported strong birefringence, indicating high molecular orientation. In this type of flow, each domain is stretched out and the molecules become aligned in the flow direction, yielding indistinguishable boundaries between domains.

Ide and Ophir have constructed a physical picture of how rodlike molecules orient in shear and elongational flow fields.³³ They have proposed that shearing does not orient molecules if the domains are stable, whereas elongational flow is strongly orienting. Baird and co-workers also found that elongational flow has a greater orienting capacity than shear flow.³⁴ Samples that had been sheared during cooling showed a higher degree of orientation, indicating that a minimum shear stress might exist for the production of orientation in shear flow. Furthermore, they observed that once orientation was produced, it could persist for a long period of time, even when samples were annealed at their softening temperature. Ophir and Ide studied the layered structure in injection-molded bars of *p*-acetoxybenzoic acid (60 mol %), terephthalic acid (20 mol %), and naphthalene diacetate (20 mol %).¹⁴ They observed four basic layers: a light skin layer, a dark subskin layer, an intermediary layer, and a dark core layer. They proposed that the skin layer originates from the fountain flow at the melt front and the subskin layer experiences mainly spreading radial flow. The intermediary and core layers originate from shearing and converging flow, respectively. They noted correctly that the morphology is also a function of distance from the gate. Williams and Garg have measured the mechanical properties of the center part of the molded HBA/HNA bars via layer removal.³⁵ They observed discrete maxima and minima in the modulus versus layer plot and proposed a three layer structure: a skin layer formed by fountain flow, an intermediary layer originating from shear flow, and a core layer due essentially to plug flow. Ide and Chung observed that the mechanical properties of extruded thermotropic copolyesters follow the general equations for fiber-reinforced composites.³⁶ In particular, their tensile strength obeys the Tsai-Hill theory and the angular dependence of the initial modulus follows the Lees equation. Some similarities in orientation between thermotropic LCPs and short-fiber reinforced polymers have been noted as follows. In short-fiber composites, Kaliske and Seifert have demonstrated the existence of layers with distinct fiber orientations in molded plaques of Nylon 6 reinforced with 33% glass fibers.³⁷ They observed a fiber-free layer next to the mold wall followed by an oriented-fiber in the flow direction; a transversely oriented layer was next followed by a flow direction oriented one; and finally in the core, another layer was observed with

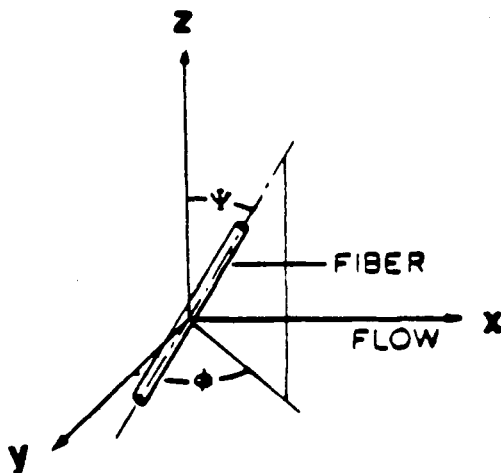


Figure 9. Schematic showing the definition of the two angles (ψ and ϕ) characterizing the orientation of the fibers.

fiber orientation perpendicular to the flow direction (see also ref 38–40).

In view of such qualitative similarities, there has been some speculation regarding modeling of the rigid rodlike domains in LCP melts as short-fiber elements in the polymeric matrix.⁴¹ Therefore we also use the treatment of fiber orientation in injection molding to interpret our experimental results. We assume that Brownian motion, which is important within a single domain, has a negligible effect on the domains as a whole. Quantitative treatments of fiber orientation are based on the equations derived by Jeffery for describing the motion of an ellipsoid suspended in an arbitrary but homogeneous flow field.⁴² The orientation of an individual fiber in three-dimensional space is characterized by the two Eulerian angles ψ and ϕ relative to a reference frame x , y , and z , as illustrated in Figure 9. In the case of two-dimensional flow, however, the motion of the particle is fully characterized by the rate of change of the angle ϕ only:

$$d\phi/dt = Z + B(d_{xy} \cos 2\phi - \frac{1}{2}(d_{xx} - d_{yy}) \sin 2\phi)$$

where Z is the vorticity and d_{ij} is a component of the rate of deformation tensor. B is a scalar related to the aspect ratio (r_p) of the particle as

$$B = (r_p^2 - 1)/(r_p^2 + 1)$$

Kenig⁴³ has proposed a qualitative model of the flow mechanisms that are responsible for fiber orientation in the observed layers using the two-dimensional Jeffery's equation.⁴² For elongational flow fields, he has used a phenomenological material parameter (λ) rather than the geometrical factor (B). This parameter which has been named the "orientability parameter" by Goettler expresses the tendency of fibers to align in the field.⁴⁴ It is always positive and can assume values both greater and less than unity. For glass fibers of 3 mm length with a volume fraction of 0.25 in an epoxy resin, Goettler has found a value of 0.80 for the orientability parameter.⁴⁴

The skin layer is formed on the passing of the melt front. The term fountain flow is used to describe the flow in which fluid elements from the core decelerate as they approach a slower moving interface and spill over toward the region vacated by the advancing interface.⁴⁵ Fountain flow is an elongational type flow in which fluid elements are elongated as they approach the mold wall. Depending on the shape of the melt front, a high degree of orientation is expected which freezes upon contact with the cold wall. Tadmore has proposed that for a circular front, a transverse orientation is expected, while for a flat front, the molecules

will align in the flow direction.⁴⁶ This is in qualitative agreement with our data; i.e., position "A" shows a high transverse orientation and other positions show high flow direction orientation in the skin layer in the xy plane. Given such high values of orientation, it seems that fountain flow is successful in stretching the polydomain structure into a monodomain structure and producing a high degree of flow direction orientation.

After the melt front has passed and the skin layer has been deposited, a converging type flow is responsible for the subskin layer. This is also an elongational flow which describes the part of flow for which the melt front exceeds the half-width of the mold, i.e., after position A. In this type of flow, the cross-section of the flow becomes smaller as the melt travels toward the end of the mold. It has been shown that the orientation is proportional to the cross-sectional area reduction to the power of $(-\lambda)$, $(\pi h/2h)^{-\lambda}$ where h is the half-width of the mold.⁴⁷ The maximum level of orientation is proposed to occur at the point where the front becomes a straight line.⁴³

$$\tan \phi_{\max} = \tan \phi_{r=h}(\pi/2)^{-\lambda}$$

If we take the average orientation function for position A as representative of $\phi_{r=h}$ and the average orientation function for the pseudoplateau (B–F) as representative of ϕ_{\max} , from the f_{xy} values of the subskin layer we can arrive at an estimate for the orientability parameter. This calculation gives an average value of 1.05 ± 0.06 for the four bands, suggesting the enhanced orientational capabilities of these materials.

At position A, the flow is radial in character and the chains are oriented transverse to the flow direction. The converging type flow, after position A, does not seem to be capable of producing a monodomain structure, probably due to a lower elongation rate as compared to fountain flow, and hence a lower degree of flow direction orientation is observed.

In the case of nonisothermal flow, the shear rate is a maximum at some distance from the skin and hence the intermediary layer may be attributed to shear flow. Liquid crystalline domains rotate in shear flow, and if they are stable no net orientation should be observed. At higher shear rates or with an increase in the stress level the domains may be broken up into a continuous phase and a stable orientation may be expected at some angle to the flow direction. The moderate flow direction orientation observed in this layer seems to confirm this mechanism and suggests that the domains may have been broken up. This is not surprising given the nonisothermal characteristics and high shear rates present in mold filling. Position A again shows a transverse orientation due to the radial character of flow in this region.

The core layer is the result of spreading radial flow which is a diverging-type flow. The melt decelerates as it diverges to fill the cavity and the chains are gradually oriented transverse to the flow direction. The spreading radial flow, like the converging-type flow, is an elongational flow, and the elongation rate does not seem to be high enough to produce a monodomain structure which would in turn produce higher degrees of transverse orientation.

Conclusions

FT-IR ATR Dichroism has proved to be a valuable technique in determining the orientation profiles in injection-molded plaques of a thermotropic main-chain LCP. Orientation functions have been measured at eight positions as a function of distance from the gate and at four positions in the thickness direction leading to a complex three-dimensional orientation profile. These orientation

profiles could explain their highly anisotropic mechanical properties.

In the *xy* plane at position A, which is the closest to the gate, molecules exhibit a transverse orientation for most layers due to the radial character of the flow in this region. Orientation functions in the thickness direction indicate that the chains are mostly planar with respect to the mold wall, especially in the skin layer. Orientation is generally decreased as the core is approached, but it is also a strong function of the location in the mold. On the basis of the orientation data in the subskin layer, a rough estimate has been made for the orientability parameter (λ): A value close to unity has been calculated that could be regarded as a phenomenological material parameter signifying the tendency of the chains to align in the flow field.

The trends observed seem reasonable in view of flow models in fiber-reinforced thermoplastics and earlier proposals regarding structural rearrangements in LCPs. Strong elongational flows such as fountain flow seem to stretch the polydomain structure into a monodomain structure, producing a high degree of orientation on the skin layer. Weaker elongational flows such as converging-type flow and spreading radial flow seem to elongate the polydomain structure but not to the point of producing a monodomain structure; the result is a lower degree of orientation in the subskin and core layers, respectively. Shear flow, with a high shear rate coupled with the non-isothermal characteristics of mold filling, seems to be able to break up the liquid crystalline domains, producing moderate flow direction orientation in the intermediary layer. While the overall features suggested by our results are in agreement with extensive electron micrographic data by Weng et al. on the same copolymer which had been molded under similar conditions,¹⁷ a complete three-dimensional orientation profile as reported here is not available in the literature. Our main objective in this work is to provide an experimental data base so as to stimulate theorists and rheologists to model the complex behavior in these materials in a more quantitative way.

Acknowledgment. This work was in part supported by ONR. We also acknowledge the helpful discussion with Drs. S. Garg and K. F. Wissbrun of Celanese Research Co., which generously supplied the samples. We extend our gratitude to Professor M. T. Shaw for helpful comments on the manuscript.

Registry No. (HBA)(HNA) (copolymer), 81843-52-9.

References and Notes

- (1) Kuhfuss, F.; Jackson, W. J., Jr. U.S. Patent 3778410, 1973.
- (2) Kuhfuss, F.; Jackson, W. J., Jr. U.S. Patent 3804805, 1974.
- (3) Calundann, G. W. U.S. Patent 4161470, 1979.
- (4) Calundann, G. W. U.S. Patent 4184996, 1980.
- (5) Mitchell, G. R.; Ishii, F. *Polym. Commun.* **1985**, *26*, 34.
- (6) Blackwell, J.; Gutierrez, G. A.; Chivers, R. A. *Macromolecules* **1984**, *17*, 1219.
- (7) Blackwell, J.; Gutierrez, G. A.; Chivers, R. A.; Ruland, W. J. *J. Polym. Sci., Polym. Phys. Ed.* **1984**, *22*, 1343.
- (8) Blackwell, J.; Biswas, A.; Bonart, R. C. *Macromolecules* **1985**, *18*, 2126.
- (9) Blundell, D. J. *Polymer* **1982**, *23*, 359.
- (10) Donald, A. M.; Windle, A. H. *Polymer* **1984**, *25*, 1235.
- (11) Donald, A. M.; Windle, A. H. *J. Mater. Sci. Lett.* **1985**, *4*, 58.
- (12) Kenig, S. *Polym. Compos.* **1986**, *7*, 50.
- (13) Jackson, W. J.; Kuhfuss, F. *J. Polym. Sci., Polym. Chem. Ed.* **1976**, *14*, 2043.
- (14) Ophir, Z.; Ide, Y. *Polym. Eng. Sci.* **1983**, *23*, 792.
- (15) Joseph, E. G.; Wilkes, G. L.; Baird, D. G. *Polym. Eng. Sci.* **1985**, *25*, 377.
- (16) Sawyer, L. C.; Jaffe, M. *J. Mater. Sci.* **1986**, *21*, 1897.
- (17) Weng, T.; Hiltner, A.; Baer, E. *J. Mater. Sci.* **1986**, *21*, 744.
- (18) Sung, C. S. P. *Macromolecules* **1981**, *14*, 591.
- (19) Hobbs, J. P.; Sung, C. S. P.; Krishnan, K.; Hill, S. *Macromolecules* **1983**, *16*, 193.
- (20) Milosevic, M., Harrick Scientific, personal communication, June, 1986.
- (21) Muramatsu, H.; Krigbaum, W. R. *Macromolecules* **1986**, *19*, 2850.
- (22) Ouchi, I.; Hosoi, M.; Shimotsuna, S. *J. Appl. Polym. Sci.* **1977**, *21*, 3445.
- (23) Flournoy, P. A.; Schaeffers, W. J. *Spectrochim. Acta* **1966**, *22*, 5.
- (24) Van Krevelen, D. W. *Properties of Polymers*, 2nd ed.; Elsevier: New York, 1976; Chapter 10.
- (25) Neff, V. D. In *Liquid Crystals and Plastic Crystals*; Gray, G. W., Winsor, P. A., Eds.; Halsted: New York, 1974; Chapter 9.
- (26) de Gennes, P.-G. *Physics of Liquid Crystals*; Clarendon: Oxford, 1974.
- (27) Gogos, C. G.; Huang, C. F. *Polym. Eng. Sci.* **1986**, *26*, 1457.
- (28) Wissbrun, K. F. *J. Rheol. (N.Y.)* **1981**, *25*, 619.
- (29) Hu, S.; Xu, M.; Li, J.; Qian, B.; Wang, X.; Lenz, R. W. *J. Polym. Sci., Polym. Phys. Ed.* **1985**, *23*, 2387.
- (30) Onogi, S.; Asada, T. *Rheology*; Astarila, A., Marrucci, G., Nicholais, L., Eds.; Plenum: New York, 1980, Vol. 1, pp 127-147.
- (31) Horio, M. *Annu. Rep. Res. Inst. Chem. Fibers, Jpn.* **1978**, *35*, 87.
- (32) Onogi, Y.; White, J. L.; Fellers, J. F. *J. Non-Newtonian Fluid Mech.* **1980**, *7*, 121.
- (33) Ide, Y.; Ophir, Z. *Polym. Eng. Sci.* **1983**, *23*, 264.
- (34) Viola, G. G.; Baird, D. G.; Wilkes, G. L. *Polym. Eng. Sci.* **1985**, *25*, 888.
- (35) Williams, G. E.; Garg, S. K. *Proc. Sec. U.S.-Jpn. Polym. Symp.* **1985**, *39*.
- (36) Ide, Y.; Chung, T. S. *J. Macromol. Sci., Phys.* **1984**, *B23*, 497.
- (37) Kaliske, G.; Seifert, H. *Plaste Kautsch.* **1973**, *22*, 837.
- (38) Darlington, M. W.; McGinley, P. L. *J. Mater. Sci.* **1975**, *10*, 906.
- (39) Murby, K. M.; Molden, G. F. *Polym. Eng. Sci.* **1977**, *17*, 843.
- (40) Folkes, M. J.; Russell, D. A. M. *Polymer* **1980**, *21*, 1252.
- (41) Chung, T. S. *Polym. Eng. Sci.* **1986**, *26*, 901.
- (42) Jeffery, G. B. *Proc. R. Soc. London, A* **1922**, *A102*, 161.
- (43) Kenig, S. *Polym. Compos.* **1986**, *7*, 50.
- (44) Goettler, L. A. *Polym. Compos.* **1984**, *5*, 60.
- (45) Rose, W. *Nature (London)* **1961**, *191*, 242.
- (46) Tadmor, Z. *J. Appl. Polym. Sci.* **1974**, *18*, 1753.
- (47) Goettler, L. A.; Leib, R. L.; Lambright, A. J. *Lub. Chem. Technol.* **1979**, *52*, 838.